Integrated thermo-poro-mechanical characterization for CO_2 Sequestration at deep aquifer conditions

Sudarshan Govindarajan[1,*], *Munir* Aldin[1], *Akshay* Thombare[1], *Omar* Abdulbaki[1], *Deepak* Gokaraju[1], *Abhijit* Mitra[1] and *Robert* Patterson[1].

[1]MetaRock Laboratories, 2703 Highway 6 S, Houston, Texas, U.S.A.

Abstract. Modelling and forecasting of injected CO_2 plume behaviour is an essential step in the baseline, monitoring, and verification [BMV] process in the CO_2 sequestration lifecycle. The goal of reduction of uncertainty through forecasting models, can be better realized by accounting for the thermo-poro-mechanical nature of the deep subsurface reservoir systems. The current study focusses on developing and refining a laboratory workflow which will help in generating representative static and dynamic datasets at ambient and deep aquifer conditions. The workflow involves characterizing the poroelastic Biot coefficient and mechanical properties at ambient, high temperatures and at reservoir representative stress conditions. This information will be combined with the dataset from a CO_2 flood experiment which replicates the displacement of brine by super critical CO_2 at ambient and high temperatures and at reservoir representative stresses. Resistivity and acoustic signals will be monitored throughout the flood experiment. Existing analytical models for fluid substitution such as the Biot-Gassmann-Brie populated with representative data will be evaluated for finding the best description of the experimental observations. The integrated results of the workflow are meant to help develop better informed static and dynamic models improving the confidence in the BMV process of CCUS.

1 Introduction

The SR15 report [1] released by IPCC in 2018 states the assumption of large-scale deployment of CO_2 removal measures to limit warming to 1.5°C by year 2100. Carbon capture, utilization, and storage (CCUS), as a CO_2 removal measure, has to implemented on a massive scale to meet the necessitated ambitious net zero emission goals. Geological storage or sequestration has the highest uncertainty through the CCUS lifecycle. Baseline, monitoring and verification programmes have been acknowledged as a fundamental and critical requirement for reducing the uncertainty in long term containment of CO_2 in the subsurface [2]. Rules promulgated by both the EPA in the US and the equivalent CO2CARE program in the EU require post injection site care satisfying strict qualification criteria, to be part of the project scope [3]. Monitorability of the storage complex is dependent on both the subsurface and the surface environment [4]. The method chosen for monitoring whether geophysical (seismic, resistivity), borehole/well based, geochemical tracing, satellite or micro-seismic based geomechanical monitoring is entirely dependent on the purpose (leak detection vs. volumetrics) as well as the geography [4, 5]. Lateral (areal) coverage for plume monitoring is enabled by surface measurements while higher resolution data can be acquired through borehole-based measurements. [4]. An integrated monitoring approach is the ideal recommendation but requires heavy investment [3, 4]. The critical reasoning and potential benefits behind investing in long term post injection monitoring as compared to higher investment in the initial characterization and preventative predictions have been compared in [3]. The inefficiency of long-term monitoring in lower certainty storage complexes due to lack of established remedial measures was pointed out in [3]. This was contrasted against the advantages of increasing certainty in the storage complexes by investing in accelerated laboratory studies, utilization of natural analogues, scaled field experiments and enhanced understanding of reservoir heterogeneity. Core analysis being the guiding standard has been the norm in the oil and gas industry. The importance of actual core-based laboratory investigations, to be used in an integrated approach with log analysis, field scale geophysical characterization and associated static-dynamic reservoir modelling is well recognized in the historical subsurface industries. This integrated approach is now being applied with greater emphasis, for increasing the certainty in the CCUS lifecycle, from the initial confidence building predictive exercises (site characterization and initial models) to establishing predictive post injection monitoring targets [3, 4, 6, 7, 8, 9, 10].

Core analysis performed at representative conditions on representative rock directly contributes to decreasing uncertainties in subsurface engineering. The comprehensive picture of the subsurface required for the numerical modelling [11] can be obtained with higher certainty when rock properties are measured at representative in-situ conditions. Deep saline aquifers are the most promising storage complexes for CCUS [8]. Characterising the displacement behaviour of the CO_2-brine systems is essential for pore space management as well as risk assessment [8, 11] The ideal integrated site characterization exercise would incorporate the high stress, pressure and temperature conditions encountered in the deep saline aquifers in the core analysis exercise. This study is a laboratory investigation of

* Corresponding author: sudarshan@metarocklab.com

the influence of in-situ conditions on CO_2 induced brine displacement and the applicable petrophysical models which help estimate the observed phenomenon.

2 Experimental Approach

The uncertainty associated with lack of understanding of rock heterogeneity at the sub seismic resolution scale leads to surprises at the field scale [12]. Geophysical monitoring data and reservoir characterization data, together, help obtain quantitative estimates necessary for verification of field behaviour against modelling estimates within uncertainty bounds [13]. Geophysical parameter behaviour is dependent on the rock minerology, porosity, pore fluid content, fluid saturations, in-situ temperatures, and pressures [14, 15]. The ability of seismic (acoustic) methods to monitor trapped CO_2 has been successfully demonstrated in the field however detecting the migrating plume front requires further investigation [16]. Prior uncertainty in petrophysical parameter estimations have a significant effect on geophysical monitorability and there is a need for accurate benchmark measurements and reservoir characterization [14]. Injecting CO_2 under supercritical conditions which can be sustained in the deep aquifers has inherent injectivity benefits [17]. The major challenge for laboratory experimental characterization for CCUS is performing the test at in-situ representative pressure and temperatures while accounting for the solubility between the supercritical CO_2 (SC-CO_2) and water and the properties of the SC-CO_2 [12]. There have been multiple studies aimed at characterizing the fluid substitution phenomenon in the lab space [12, 14, 15, 16, 17, 18, 19, 20, 21]. To replicate CO_2 injection into the deep aquifers, most approaches involved injecting dry CO_2 gas or CO_2-brine solutions into brine saturated rock samples at varied conditions of temperature, pressure, and usually low effective stresses. Experimental observations were obtained through either isolated or combined acoustics, CT scanning and resistivity-based monitoring methods. The current investigation employs the porous plate technique and incorporates injection of dry SC-CO_2 into a brine saturated rock at reservoir representative stress, temperature, and pressure conditions while measuring the resistivity during the entire duration of the experiment. The porous plate technique is a reliable method for replication of the typical distribution of fluids in reservoir rocks [22,23]. Electrical/electromagnetic based surveys have been found to be a good complement to seismic measurements in the field as resistivity is more sensitive to saturation changes than compressional velocities [13]. Resistivity measurements in the lab have been found to be more reliable using the porous plate technique when performed at very slow injection rates following steady state equilibration protocols and a coherent brine saturation – resistivity index measurement is critical for validating logs by developing higher accuracy in fluid saturation definitions [22].The current study adopts a modification of the established I-S_W protocol by injecting at slow flow rates and using the porous plate for preferential effluent expulsion. The current study also incorporates typical reservoir representative high effective stress conditions for greater reduction in uncertainty.

3 Theoretical Background

Supercritical fluids have the advantage of having low viscosity and relatively low compressibility (Appendix A) [24]. Injecting a material in the supercritical state enables maximising the pore space available in the subsurface. The study of the displacement of brine by non-wetting fluid using the single sample-water wet membrane, porous plate technique following Archie's equations is well established in the industry [22]. The porous plate acts as a barrier to the non-wetting fluid and allows for gradual development towards irreducible water saturations. The resistivity being monitored during this gradual displacement can be plotted in a log-log plot against the water saturation (I-S_W plot) for obtaining the saturation exponent, "n". The saturation exponent has been historically estimated for typical lithologies and reliable ranges for associated saturation exponents have been made. The I-S_W plot is a reliable indicator of the saturation state of the sample. In the present study the brine in the samples is displaced by SC-CO_2 while monitoring the resistivity and the deviation from linearity in the I-S_W plot is used as an indicator of breakthrough or end of experiment. Fig. 1 shows an example of a typical I-S_W plot.

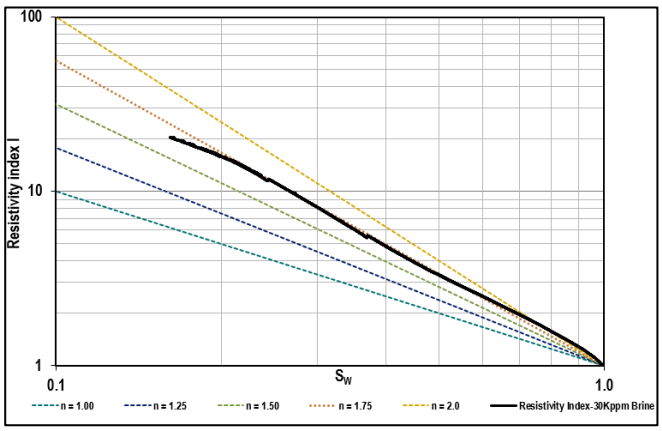

Fig. 1. Resistivity Index Vs. water saturation on log-log plot.

Fluid substitution as a phenomenon occurring during subsurface engineering has been well addressed by the hydrocarbon industry [25]. The general formula for the saturated porous system bulk modulus can be represented as under:

$$K_{SAT} = K_{dry} + \frac{(1-(K_{dry}/K_0))^2}{(\varphi/K_F)+((1-\varphi)/K_0)-(K_{dry}/K_0^2)} \quad (1)$$

where,
K_{SAT}: Bulk modulus of saturated porous medium
K_{dry}: Drained Bulk modulus
K_0: Grain modulus = Skeletal modulus = Mineral bulk modulus
K_F: Fluid Bulk modulus
Φ: Porosity as a fraction
The velocity can then be calculated as:

$$V_{PSAT} = \sqrt{\frac{1}{\rho_{sat}} * (K_P + K_{dry} + \mu\frac{4}{3})} \quad (2)$$

where,

$$K_P = \frac{(1-(K_{dry}/K_0))^2}{(\varphi/K_F)+((1-\varphi)/K_0)-(K_{dry}/K_0^2)} \quad (3)$$

V_{PSAT}: Saturated compressional velocity
ρ_{SAT}: Density of saturated rock
μ: G = Shear modulus of rock
Theoretically, the shear modulus for a rock is the same irrespective of saturated or dry condition as the fluids have zero shear velocity. The above equations have been utilised previously such as in reference [18] for interpreting laboratory measurements. However, the critical points mentioned in reference [25] are, that the above formulation was defined for seismic frequencies and may not work as well at the laboratory ultrasonic (1MHz) scale and that the K_{dry} has to be the drained bulk modulus i.e., either at constant pore pressure with free flow of fluid or with pore pressure drained to atmospheric condition in the absence of pore fluid. Reference [17] illustrated another expression for the undrained bulk modulus for a fluid saturated rock as:

$$K_U = K_{dry} + \frac{\alpha^2}{(\varphi/K_F)+((\alpha-\varphi)/K_0)} \quad (4)$$

where,
K_U: undrained bulk modulus of saturated porous medium
α: Biot poroelastic coefficient which is given by:

$$\alpha = 1 - (K_{dry}/K_0) \quad (5)$$

The fluid bulk modulus may be defined for a finely mixed fluid system by the Reuss average (parallel formulation):

$$\frac{1}{K_F} = \sum \frac{S_i}{K_i} \quad (6)$$

The fluid bulk modulus for a patchy saturation can be expressed by the Voigt average (series formulation) as:

$$K_F = \sum S_i * K_i \quad (7)$$

It was also shown in [17] that the Biot-Gassmann-Brie formulation was able to best describe the experimental observations.

$$K_F = S_B^N * K_B + (1 - S_B^N) * K_{CO_2} \quad (8)$$

where:
S_i: saturation of i^{th} component
K_i: Bulk modulus of i^{th} component
K_B: Brine modulus
S_B: Brine saturation
K_{CO2}: Bulk modulus of CO_2
The combined saturated density of the porous solid filled with the mix of fluids can be estimated as

$$\rho_{SAT} = \rho_{dry} + (\varphi) * \rho_F \quad (9)$$

where:
ρ_{dry}: Dry Bulk density of sample

$$\rho_F = S_B * \rho_B + (1 - S_B) * \rho_{CO_2} \quad (10)$$

where:
ρ_B: Density of brine at temperature, pressure
ρ_{CO2}: Density of CO_2 at temperature, pressure

4 Experimental System Overview

Prolonged experiments with SC-CO_2 at high temperatures and pressure require specialised equipment. The rock mechanics testing system, shown in Fig. 2 has been modified to contain the SC-CO_2 without any leaks. The system consists of a servomechanical frame press capable of reaching up to 300,000 lbs within an isothermal enclosure. The confining pressure pump has multivariable control capability and can apply up to 30000 psi (2068 MPa) with μ-inch resolution. The pore pressure pumps are 30 cc pumps capable of reaching 15000 psi (103 MPa) with nano-inch resolution. The pore pressure pumps can handle SC-CO_2 and have the necessary higher resolution to address the volume monitoring for saturation estimations. The system has also been modified with requisite channels for making the resistivity measurements. The system has also been modified with a high-resolution acoustics monitoring system, shown in Fig. 3 for live acquisition and display of the compressional velocity data as noted in [26].

Fig. 2. Rock Mechanics Test Equipment.

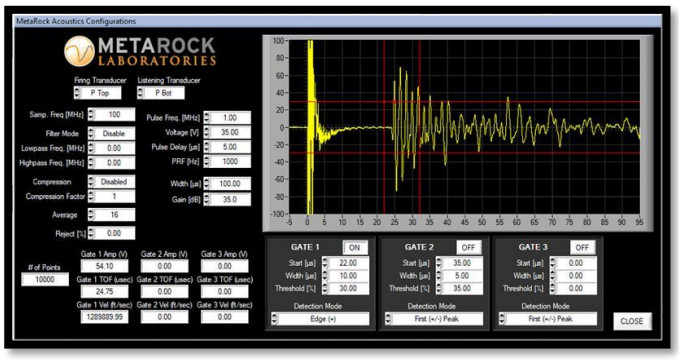

Fig. 3. Data acquisition and monitoring system for live high resolution compressional wave acoustics data.

Ultrasonic (1MHz) acoustic transducers are isolated from pressure and housed within the endcaps. The system is also rated for achieving high temperatures up to 450°C (842F) with acoustic measurement achievable up to 200°C (392F).

5 Experimental Suite, Results and Discussion

5.1. Testing Suite Design and Sample Statistics

The testing suite was defined to address the input requirements for the equations that govern the fluid substitution challenge. The poroelastic coefficient, the dry bulk modulus and the grain modulus are all required inputs. Additional triaxial testing at saturated condition was performed to be able to establish the range of expected velocity variation. The SC-CO_2 flow testing was performed on Buff Berea sandstone at ambient 35°C (95F) and higher temperature of 65°C (149F). Samples belonged to the same outcrop block and were prepared to be approximately 1" in diameter and 2" in length meeting all recommended ASTM/ISRM standards. The permeability range of the sample as obtained from the outcrop database was between 150-350 mD brine (KCl) permeability and 400-500 mD Klinkenberg permeability with N_2 gas. Grain volume and bulk volume of the samples were also measured to ensure uniformity. Table 1 shows the detailed statistics for the sample set.

Table 1.Sample Statistics

Sample Detail	Mean	Std Dev	Coefficient Of Variation
Length (in)	1.997	0.004	0.182
Diameter (in)	0.994	0.001	0.088
Weight (g)	51.074	0.177	0.347
Bulk Volume (cc)	25.507	0.048	0.186
Grain Volume (cc)	19.261	0.066	0.341
Pore Volume (cc)	6.246	0.085	1.361
Grain Density (g/cc)	2.651	0.001	0.056
Bulk Density (g/cc)	2.002	0.008	0.385
Porosity (%)	24.489	0.307	1.253

5.2. Triaxial testing with static and dynamic characterization:

All testing was performed at a high effective stress of 2000 psi (13.78 MPa). Triaxial tests were carried out for the characterization of the dry bulk modulus at both temperature conditions, at confining pressure of 2000 psi (13.78 MPa), under drained conditions, at slow loading rates. The differential stress cycles were unloaded at approximately 7000 psi (48.26 MPa) without taking the sample to failure. Compressional and shear velocities were acquired throughout the duration of the test. Results from the base triaxial testing are displayed from Fig. 4 to Fig. 7. The comparison between the axial and radial strain responses at 35°C (95F) and 65°C (149F) indicate that Buff Berea (being a quartz-rich rock) does not display a marked change in deformation behaviour within that temperature range. However, the compressional and shear velocities are both slightly lowered with the increase in temperature. The choice of 65°C (149F) was done as sandstones do not exhibit significant changes in elastic properties between 25°C (77F) to 45°C (113F) [27], however even at 65°C (149F) we did not observe significant change in the mechanical and acoustic properties.

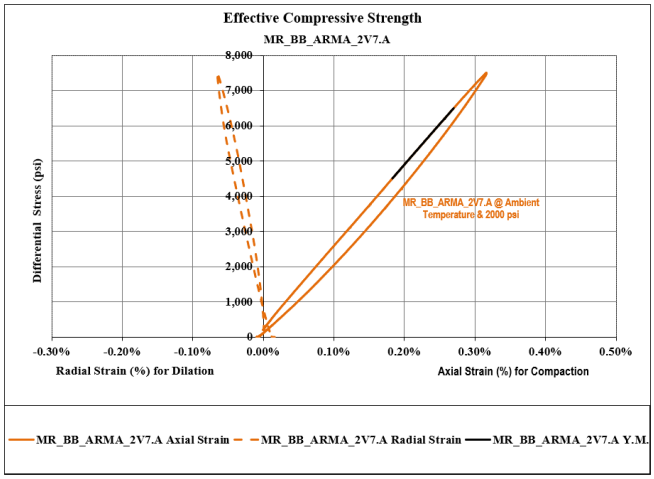

Fig. 4. Stress-strain plot for the ambient (35°C) temperature triaxial test and confining pressure of 2000 psi.

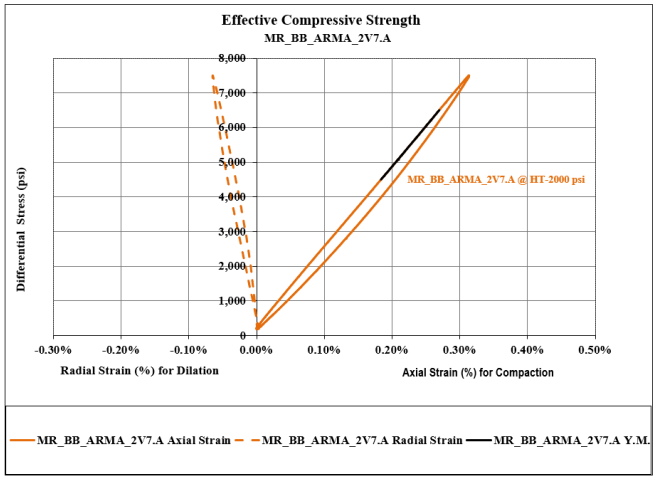

Fig. 5. Stress-strain plot for the high (65°C) temperature triaxial test and confining pressure of 2000 psi.

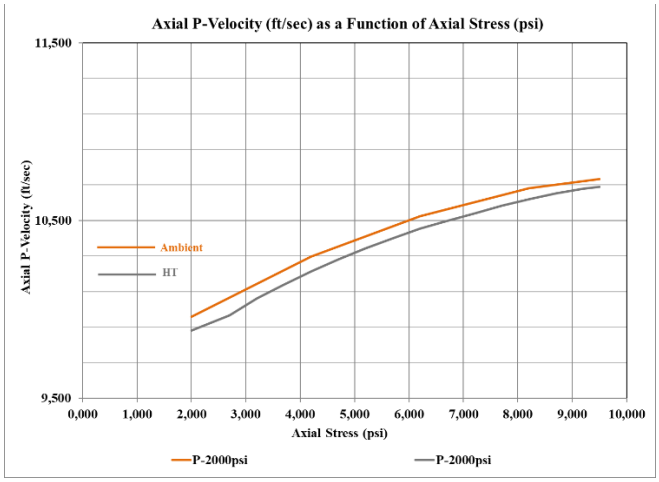

Fig. 6. Compressional velocity comparison at ambient and high temperature.

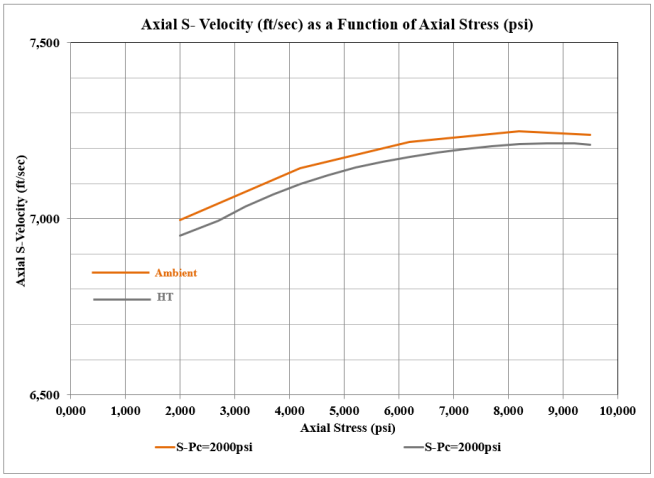

Fig. 7. Shear velocity comparison at ambient and high temperature.

5.3. Poroelastic characterization:

Poroelastic coefficient characterization as per reference [28], was carried out by cycling confining and pore pressures while maintaining the effective stress of 2000 psi (13.78 MPa). Fig. 8, Fig. 9 display the summary and results of the poroelastic coefficient characterization.

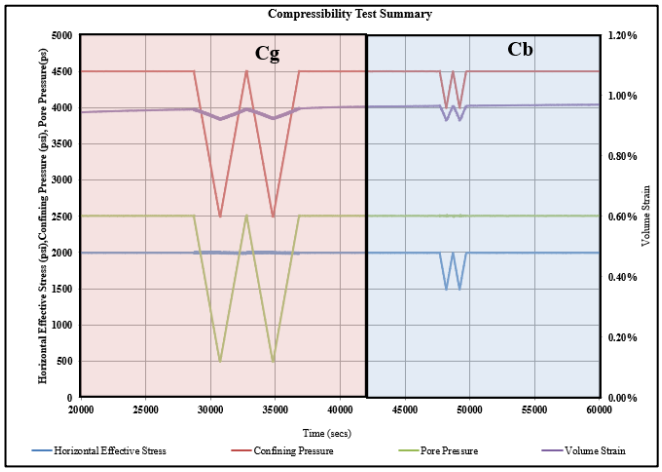

Fig. 8. Poroelastic coefficient measurement experimental summary.

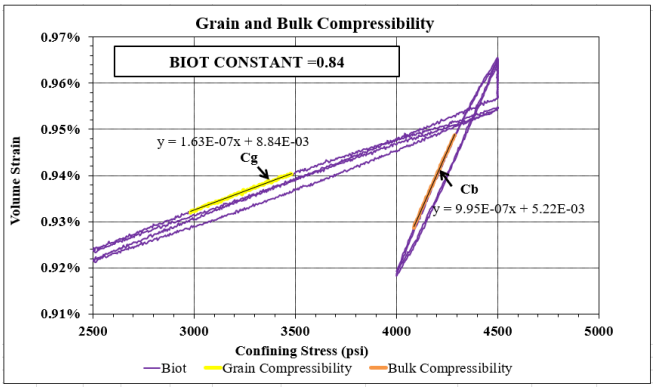

Fig. 9. Experimental results for poroelastic coefficient measurement.

5.4. SC-CO_2 flow study:

5.4.1 Set-up and experimental conditions

The fluid substitution experiment was carried out on two different plugs at ambient and high temperature. The protocol for both involved saturating the sample with brine at stress and flowing SC-CO_2 from the top to the bottom with the porous plate positioned at the bottom end. Fig. 10 shows the simplified flow schematic for the fluid substitution experiment.

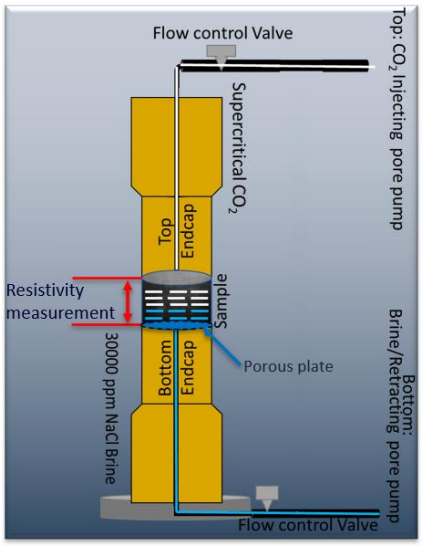

Fig. 10. Simplified flow schematic for the fluid substitution experiment.

Resistance and compressional velocity were monitored throughout the duration of the experiment. Experiments were performed maintaining an effective stress of 2000 psi (13.78 MPa) with confining pressure at 4500 psi (31.02 MPa) and pore pressure at 2500 psi (17.236 MPa). Samples were initially saturated with 30000 ppm NaCl brine at 100 psi pore pressure and confining of 2000 psi (13.78 MPa). The conditions were then progressed to desired experimental conditions of 4500 psi (31.02 MPa) confining and 2500 psi (17.236 MPa) pore pressure at stabilized temperature. Once stabilization was achieved (strain and pore pressure), injection of SC-CO_2 was begun from the top. The total experiment ran for 150 hours approximately. The ideal porous plate I-SW experiment is meant to be performed at very low flow rates of one pore volume over 10-30 days. The injection of the SC-CO_2 results in the creation of differential pressure across the sample. It is recommended to displace the fluid/brine saturating the sample at a constant injection rate with super critical fluids.

The injection is to be done while monitoring resistivity change across the sample along with ultrasonic velocity and the differential pressure across the sample. This investigation studied the use of the differential pressure as a feedback channel for driving the injection in the interest of expediency.

As the injection was begun, initial differential pressure created was around 50 psi (2550 at upstream and 2500 psi at downstream). Once flow stabilized at this differential pressure the system was programmed to respond with flow

rates necessary to maintain a differential pressure of 150 psi. The limiting differential pressure for the experiment, is the differential pressure sustainable across the porous plate which was approximately 200 psi. When injection is started, some time is consumed in establishing an interface between the SC-CO_2 and the brine and there is a delay in the downstream pump response to the upstream pump. The dead volumes within the system must be thoroughly defined to enable higher accuracy in the pump volume-based saturation definitions.

5.4.2 Saturation based on volume and resistivity monitoring:

The volume of effluent brine on the downstream side was deemed as indicative of saturation conditions within the sample. The results of the ambient temperature fluid substitution experiment are shown in Fig. 11 to Fig. 13**Fig. *13***. The injection was carried out by gradually increasing the desired differential pressure setpoint across the sample. The resistivity was measured across the whole sample in the axial plane. Brine is a conductive fluid. The replacement of the brine in the sample by SC-CO_2 results in the increase in the resistivity of the sample. The time at which the resistivity starts increasing is indicative of sample penetration by the SC-CO_2. The resistivity changed from an initial 5.357 (Ω-m) to 24.787 (Ω-m) which is an increase of 362.7%. The I-Sw plot Fig. 13 indicates that the saturation exponent for the Buff Berea sandstone is 2. This is a value typically expected for sandstones. The measured resistivity across the sample increases exponentially when no more brine is expelled from the bottom of the sample while SC-CO_2 injection is being continued. This could indicate either breakthrough by the SC-CO_2 or achieving residual saturations for that rock type. The ideal I-SW experiment implemented at very low injection rates would entail piston-like uniform displacement of the wetting fluid by the non-wetting fluid. However, since SC-CO_2-brine interactions could entail mixing of the two fluids to some degree, ideal piston like uniform displacement is not expected. The utilization of the differential pressure as a driving mechanism also resulted in relatively higher instantaneous flow rates. The I-SW for the ambient temperature experiment displays deviation from linearity at 48% brine saturation indicating rapid increase in resistivity. The phenomenon was also reflected in the reduced brine effluent volumes and the cessation of the retraction of the downstream pump. Based on the resistivity behaviour, the pump movement and effluent volumes, the residual saturation of water at the end of the experiment is deemed to be approximately 48%.

The current study utilized 30000ppm NaCl brine. The possibility of salt precipitates being left behind as the brine is displaced or due to interaction between brine and dry SC-CO_2 exists, however it was not observed in the current experiment based on visual inspection. Further investigation in the form of thin section analysis or XRD is needed to be performed for increasing confidence in the observation. The phenomenon of salt precipitation is of greater importance in high salinity brines and should be taken into consideration after formation water evaluation.

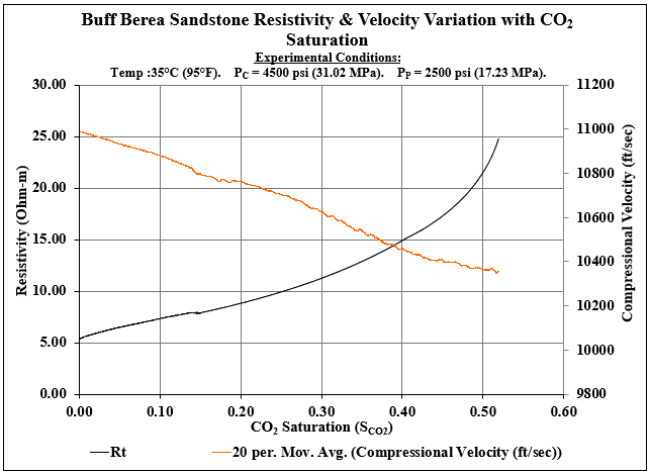

Fig. 11. Resistivity and velocity variation due to fluid displacement at ambient temperature.

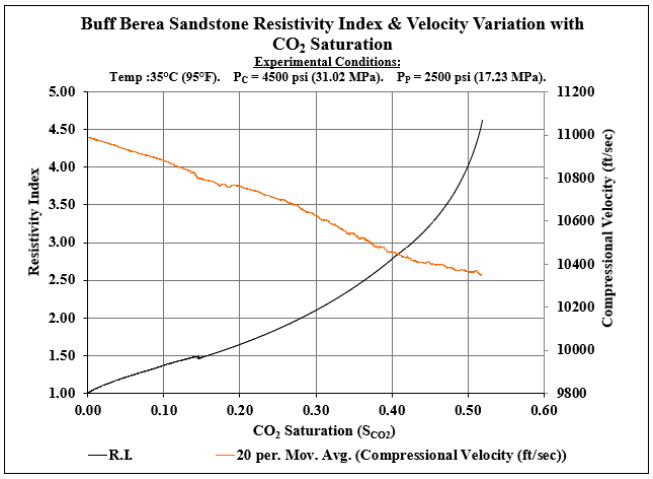

Fig. 12. Resistivity Index and velocity variation due to fluid displacement at ambient temperature.

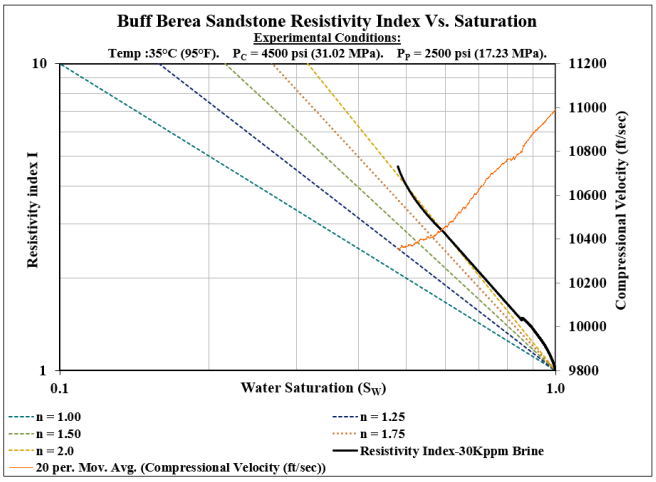

Fig. 13. I-Sw plot for brine displacement by SC-CO_2 at ambient temperature.

5.4.3 Acoustic monitoring:

Brine has greater density than SC-CO_2 under the established experimental conditions. As the brine gets displaced and volume of SC-CO_2 within the sample increases there is a

decrease in the bulk density and modulus of the porous rock system. This decrease causes a decrease in the measured compressional velocity across the sample. The compressional velocity changed from an initial 10991 ft/sec to 10325 ft/sec which is a 6.44% change. This is similar to results obtained by [17], [18] and [27]. Greater decreases in velocities have been observed in carbonates but at lower effective stresses [16]. The sensitivity of acoustic measurements to change in fluid in the samples, were observed, at low effective stresses of 453 psi (3 MPa) and 290 psi (2 MPa) in [18] and [17] respectively. The acoustic data was found to be sensitive to change in water saturation for up to 10-20% S_W by [18] and up to 25% S_W by [17]. In the present study the effective stress utilised was 2000 psi (13.78 MPa). The high-resolution equipment enabled capture of acoustic data at the rate of a measurement every second. The sensitivity of the velocity seemed to be damped only at around 40 % saturation of SC-CO_2 i.e., after displacement of 40% of original brine volume. The different models for fluid substitution were compared against the measured experimental data. Fig. 14. shows the comparison of the different estimates with an averaged curve representing the high resolution, high volume acoustic dataset. The Reuss and Voigt based velocity predictions form the lower and upper bounds respectively for the experimental measurement. The velocity calculated using the modified Voigt i.e., the Biot-Gassmann-Brie expression matches very closely with the measured velocities. The absolute error when comparing the velocity calculated using the Reuss based parallel formulation for finely mixed fluids and the experimental measurements comes to a minimum of 0.01% and a maximum of 5.16%. The absolute error when comparing the velocity calculated using the Voigt based series formulation for patchy saturation and the experimental measurements comes to a minimum of 0.16% and a maximum of 1.7%. The absolute error when comparing the velocity calculated using the modified Voigt i.e., the Biot-Gassmann-Brie based series formulation for patchy saturation and the experimental measurements comes to a minimum of 0.49% and a maximum of 0.82%. The meandering nature of the experimental velocity curve indicates that the fluid distribution is more complicated than can be estimated by the Reuss and Voigt bounds, similar to [17]. The exponent value utilised for the Biot-Gassmann-Brie was 1.25. Even though the Biot-Gassmann-Brie curve matches well, it can still be seen that the experimental curve oscillates between indicating a mixed or patchy saturation. The overall trend in this case is more towards a series displacement which may be the result of the utilization of the porous plate technique. Since the maximum error was found to be between the Reuss or parallel formulation and the experimental measurement, a modification similar to the Biot-Gassmann-Brie is proposed as below:

$$K_F = \frac{K_B * K_{CO2}}{K_B * (1 - S_B^m) + K_{CO2} * S_B^m} \qquad (11)$$

where:
K_B: Brine modulus
S_B: Brine saturation
K_{CO2}: Bulk modulus of CO_2
m: modified Reuss exponent

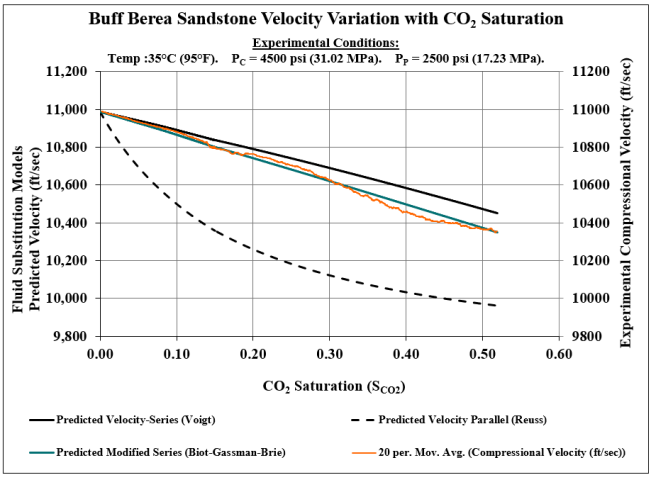

Fig. 14. Comparison of experimental measurement and velocity estimates using different models.

Fig. 15 shows the comparison of the velocity estimate based on the modified Reuss formulation with an "m" value of 0.3. The absolute error when comparing the velocity calculated using the modified Reuss based formulation and the experimental measurements comes to a minimum of 0.05% and a maximum of 1.48%. This enables a reduced uncertainty in the velocity estimate window.

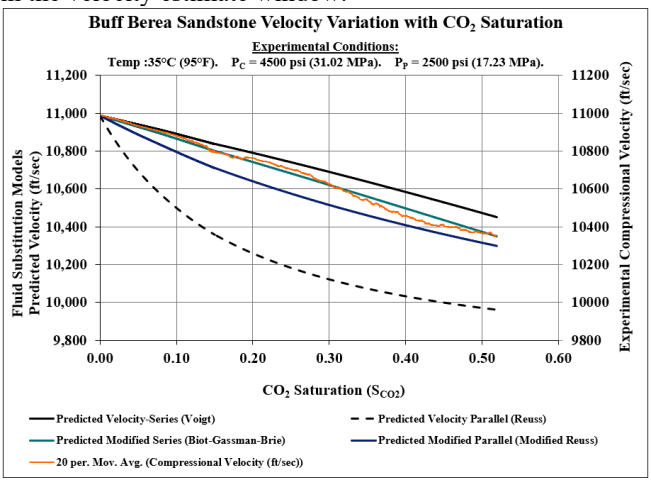

Fig. 15. Modified Reuss based velocity estimate comparison with experimental data.

5.4.4 Failure Envelope Characterization:

After completion of the fluid substitution testing, the same sample was utilised to conduct a multistage triaxial test as per [29]. The samples used for the current study were companion samples used for [29]. [29] had generated a Mohr Coulomb failure envelope based on multiple single stage triaxial testing. Fig. 16 shows the failure envelope and strength data for the fluid substitution sample and Fig. 17 displays the finalized failure envelope and strength data for the virgin Buff Berea sandstone samples. The unconfined compressive strength (U.C.S.) estimate for room temperature testing on virgin samples was 5929.7 psi and that on SC-CO_2 exposed sample was 4518 psi. This indicates a reduction of U.C.S. by 24%. The cohesion for the virgin samples was 1288.3 psi and the SC-CO_2 exposed sample exhibited 1058.4 psi. The reduction in cohesion was 18%. The friction angle changed

from 42.33° for the virgin sample to 39.7°, a change of 6%. The fluid substitution samples did undergo a lot of processes such as saturation and desaturation along with exposure to CO_2 at high effective stress and pore pressure. However, most of those process steps are meant to reproduce the processes seen in the field. As such the difference in strength properties can be taken to be reasonably representative.

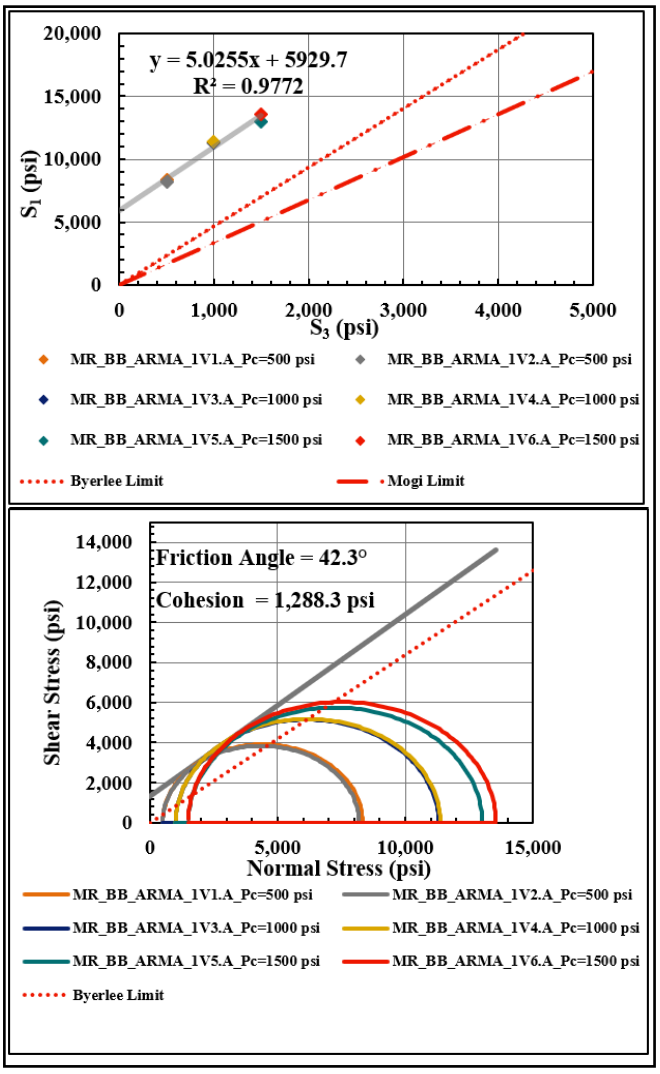

Fig. 16. Mohr Coulomb failure envelope and U.C.S. estimate for Buff Berea Sandstone.

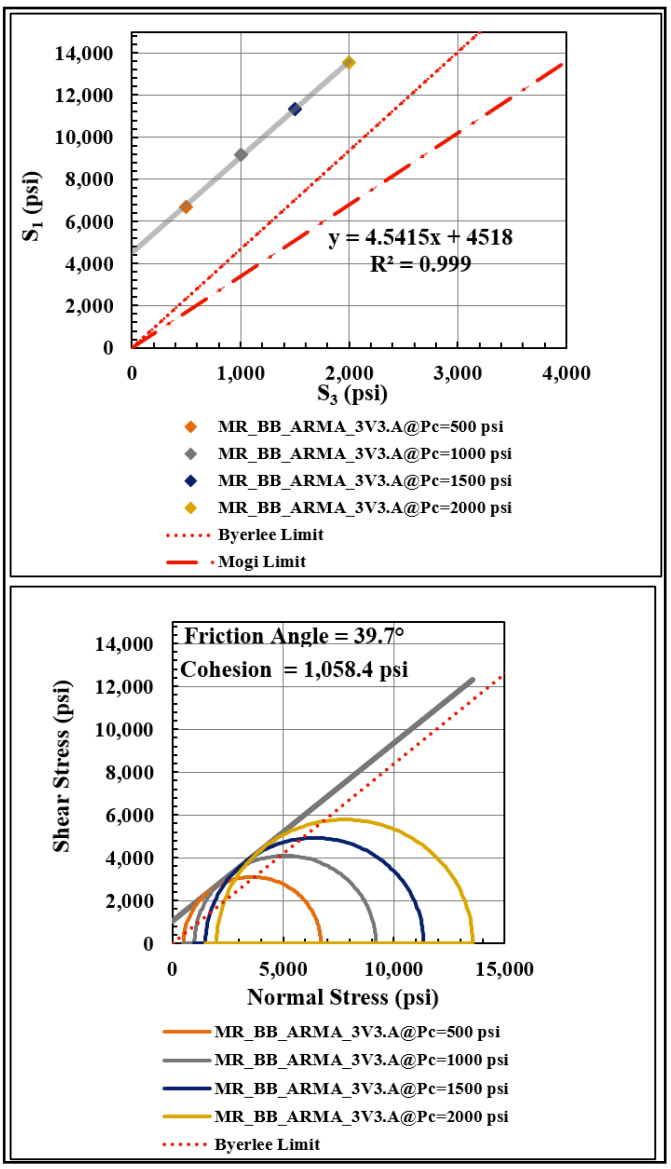

Fig. 17. Multistage triaxial test results on the fluid substitution sample tested at ambient temperature.

The high temperature fluid substitution experiment for the companion Buff Berea sample is summarised in Fig. 18.

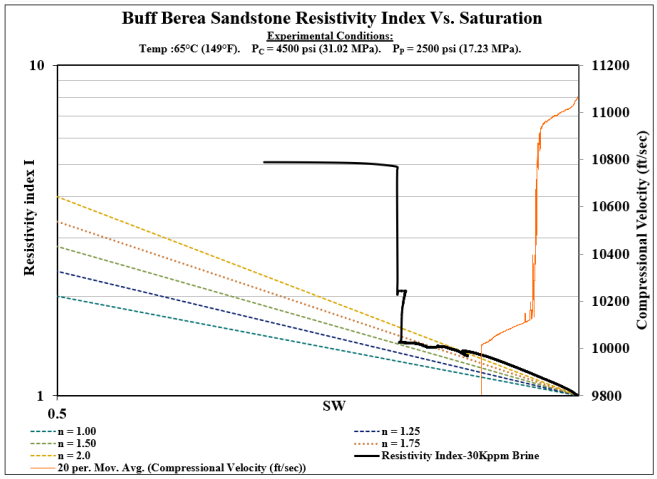

Fig. 18. 65°C (149F) fluid substitution -high injection rate induced breakthrough of SC-CO_2

The injection of the SC-CO_2 in the experiment was driven by the differential pressure across the sample. However, the selected setpoint for the differential pressure initiated a very high flow rate which caused a breakthrough of the SC-CO_2 through the sample. Fig. 19. illustrates an example of gradual sustained injection in a carbonate rock at high temperature of 120°C (248F) and high effective stress of 2500 psi (17.23 MPa). Resistivity index trend in the I-SW plot seems to indicate that the water saturation at the end of the experiment is 0.4 or 40%. The saturation exponent for the SC-CO_2 induced brine displacement through the rock is 1.75. The carbonate sample didn't have any companion samples for performing the triaxial and poroelastic coefficient characterizations required for the velocity predictions which were consequently not evaluated.

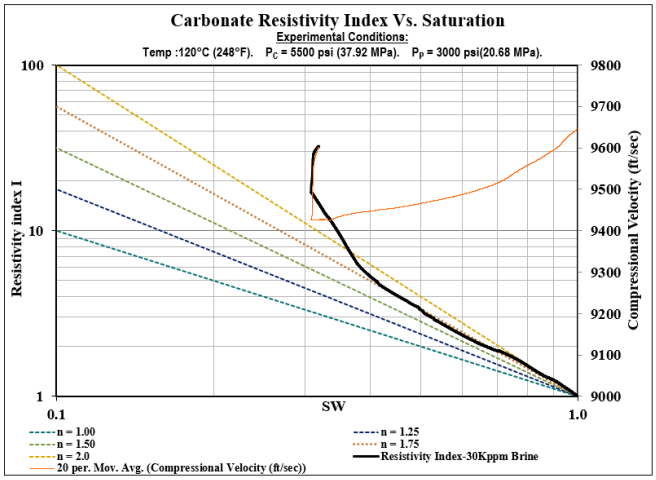

Fig. 19. High temperature, high pressure fluid substitution in carbonate sample.

6 Conclusions

Implementing an integrated, robust, laboratory program for addressing CCUS challenges helps reduce modelling and field scale uncertainty. The Biot-Gassmann-Brie formulation helps predict the acoustic behaviour during laboratory fluid substitution experiment reasonably well. The proposed modified Reuss formulation helps narrow the window for the model-experimental data match.

Appendix A: CO_2 Reference Data

All reference data has been sourced or calculated based on information from [32]. The critical temperature for CO_2 is 30.97°C, the critical pressure is 1070 psia and critical density is 0.467 g/cc. Fig. 20 to Fig. 22 show the variation of density, viscosity and compressibility of CO_2 with increase in pressure under different isothermal conditions of 30°C, 35°C and 65°C. At any temperature, with increase in pressure, phase change is observed. The critical point marks the transition to supercritical phase. Fig. 20 illustrates that in the gaseous phase, at lower pressures, the maximum magnitude of the density only reaches around 0.35 g/cc. In the supercritical phase, at all three temperatures, the densities are much higher. At 35°C, the density of the supercritical phase, is very close to the density of liquid CO_2 at 30°C. The region of interest (2500 psi) for the current study is marked in a red rectangle. The densities displayed by CO_2 in the supercritical phase are closer to liquid densities than gaseous densities especially with increase in pressure. The viscosity in the supercritical phase decreases with increase in temperature and remains lower than liquid phase viscosities at all pressures and temperatures. The compressibility shown in Fig. 22 has been calculated from density and velocity data as below:

$$C_{b=}\frac{1}{c*\rho*V_P^2} \quad (12)$$

Where: ρ: Density in kg/m^3

V_P: Compressional velocity in m/s

c: 1.4504E-04 (conversion to psi)

Fig. 22 illustrates that the compressibility of CO_2 at higher pressures in the supercritical phase is closer to liquid compressibility than gaseous compressibility.

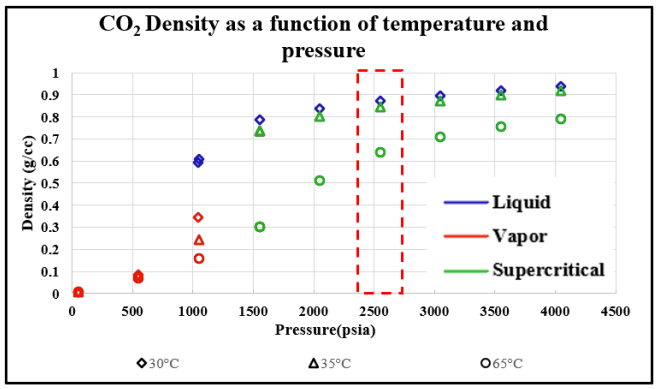

Fig. 20. Change in density of CO_2 as a function of pressure increase at three isothermal conditions of 30°C,35°C and 65°C. Phase change is mapped by colour coding.

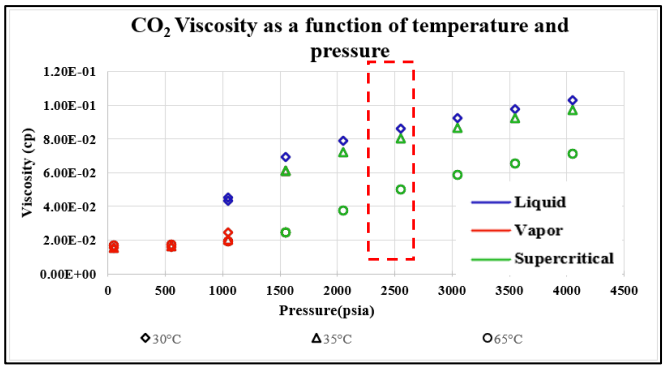

Fig. 21. Change in viscosity of CO_2 as a function of pressure increase at three isothermal conditions of 30°C,35°C and 65°C. Phase change is mapped by colour coding.

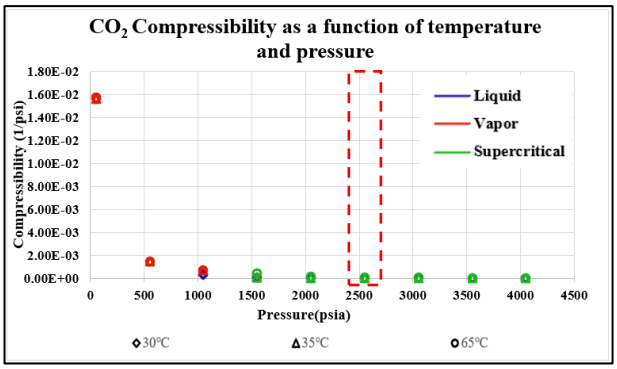

Fig. 22. Change in compressibility of CO_2 as a function of pressure increase at three isothermal conditions of 30°C,35°C and 65°C. Phase change is mapped by colour coding.

Authors would like to acknowledge the guidance of the late William Mickelson and the kind help of Hamad Aldin, Malik Al Salman, Hatim Aldin and Sneha Kalidindi in the execution of the experimental program.

References

1. Masson-Delmotte, V., P. Zhai, H.-O. Pörtner, D. Roberts, J. Skea, P.R. Shukla, A. Pirani, W. Moufouma-Okia, C. Péan, R. Pidcock, S. Connors, J.B.R. Matthews, Y. Chen, X. Zhou, M.I. Gomis, E. Lonnoy, T. Maycock, M. Tignor, and T. Waterfield. *IPCC, 2018: Global Warming of 1.5°C. An IPCC Special Report on the impacts of global warming of 1.5°C above pre-industrial levels and related global greenhouse gas emission pathways, in the context of strengthening the global response to the threat of climate change, sustainable development, and efforts to eradicate poverty.* In press.
2. A. Simone, E. Mackie and N. Jenvey, En. Proced. **1**, *GHGT-9*, 2219-2226, (2009).
3. S. D. Hovorka, En. Proced. **114**, *GHGT-13*, 3754-3756, (2017).
4. M. Smith, D. Campbell, E. Mckay, and D. Polson, *CO_2 aquifer storage site evaluation and monitoring*. Herriot-Watt University, Edinburgh (2011).
5. S. Carrol, K. Mansoor, X. Yang, T. A. Buscheck and Y. Sun. En. Proced. **114**, *GHGT-13*, 3628-3635, (2017).
6. K. Yamamoto. *CO2SC Symposium.*26-28, (2006).
7. J. Desroches, L. Jammes, and T. Berard. *CO2SC Symposium.*238-241, (2006).
8. S. Bachu and B. Bennion. *CO2SC Symposium.*193-195, (2006).
9. DOE-NETL, *BEST PRACTICES: Site Screening, Site Selection, and Site Characterization for Geologic Storage Projects* (2017). DOE/NETL-2017/1844.
10. J. Rutqvist, J. Birkholzer, and C.F. Tsang. *CO2SC Symposium.*230-232, (2006).
11. *DOE-NETL, BEST PRACTICES: Risk Management and Simulation for Geologic Storage Projects (2017). DOE/NETL-2017/1846*
12. R. Pini, S. Krevor. Chapter 7-Laboratory studies to understand controls on Flow and Transport for CO_2 storage. Editors, P. Newell, A. G. Ilgen. *Science of Carbon Storage in Deep Saline Formations*. Elsevier, pp 145-180, (2019).
13. B. Dupuy, A. Romdhane, P. Eliasson, H. Yan. Combined geophysical and rock physics workflow for quantitative CO2 monitoring. International Journal of Greenhouse Gas Control,106, 103217, (2021).
14. Z. Xue, T. Ohsumi, H. Koide.An experimental study on seismic monitoring of a CO2 flooding in two sandstones. Energy,30, 2352-2359, (2005).
15. A. JafarGandomi, A. Curtis. Assesing the monitorability of CO2 saturation in subsurface saline aquifers. International Journal of Greenhouse Gas Control.**7**. pp 244-260.(2012)
16. V. Vilarrasa, R.Y. Makhnenko, J. Rutqvist, Chapter 9 - Field and Laboratory Studies of Geomechanical Response to the Injection of CO2, Editor(s): P. Newell, A. G. Ilgen, *Science of Carbon Storage in Deep Saline Formations*, pp 209-236, Elsevier,(2019).
17. M. Gutierrez, D. Katsuki, A. Almarabat. Seismic velocity change in sandstone during CO2 injection. E3S Web of Conferences, 205, ICEGT (2020).
18. J. Kim, T. Matsuoka, Z. Xue. Monitoring and detecting CO_2 injected into water-satuated sandstone with joint seismic and resistivity measurements. *Exploration Geophysics*, 42, 58–68, (2011).
19. I. Falcon-Suarez, H. Marin-Moreno, F. Browning, A. Lichtschlag, K. Robert, L. J. North, A.I. Best. Experimental assesment of pore fluid distribution and geomechanical changes in saline sandstone réservoirs during and after CO2 injection.
20. T. Tsuji, T. Ikeda, F. Jiang. Hydrologic and elastic properties of CO_2 injected rock at various reservoir conditions : Insight into quantitative monitoring of injected CO_2. En. Proced. **114**, *GHGT-13*, 4047-4055, (2017).
21. H. Ott, S. Berg, S. Oedai. Displacement and mass transfer of CO_2/Brine in sandstone. *International Symposium of Society of Core Analysts.* SCA2011-05. (2011).
22. M.Z. Kalam, K.Al. Hammadi, O.B. Wilson, M. Dernaika and H. Samosir. Importance of porous plate measurements on carbonates at peseudo reservoir conditions. *International Symposium of Society of Core Analysts.* SCA2006-28, (2006).
23. D.G. Longeron, M.J. Argaud and L. Bouvier. Resistivity Index and capillary pressure measurements under reservoir conditions using crude oil. 64th Annual Technical Conference and Exhibition of the Society of Petroleum Engineers. (1989).
24. Richard Rosen, William Mickelson, Munir Sharf-Aldin, Basak Kurtoglu, Tobi Kosanke Meghana PaiAngle, Robert Patterson, Faraz Mir, Santhosh Narasimhan, and Amir Amini. Impact of Exp Studies on Unconventional Mechanisms.SPE-168965. SPE Unconventional Resources Conference – USA held in The Woodlands, Texas, USA, 1-3 April, (2014).
25. G. Mavko, T. Mukerji, J. Dvorkin. *The Rock Physics Handbook***.** pp 266-339. (2009).

26. D. Gokaraju, M. Aldin, A. Thombare, A. Mitra, S. Govindarajan, R. Patterson. A novel method for experimental characterization of the Poroelastic Constants in Unconventional formations.URTeC :2902907, (2018).
27. V. Mikhaltsevitch, M. Lebedev, and Boris Gurevich. Measurements of the elastic and anelastic properties of sandstone flooded with supercritical CO_2. Geophysical Prospecting, **62**, pp 1266–1277, (2014).
28. J. W. Dudley, M. Brignoli, B. R. Crawford, R. T. Ewy, D. K. Love, J. D. McLennan, G. G. Ramos, J. L. Shafer, M. H. Sharf-Aldin, E. Siebrits, J. Boyer, M. A. Chertov. ISRM Suggested Method for Uniaxial-Strain Compressibility Testing for Reservoir Geomechanics. Rock Mech Rock Eng **49,** pp 4153-4178, (2016).
29. S. Govindarajan, M. Aldin, A. Guedez, A. Thombare, D. Gokaraju, A. Mitra, R. Patterson. Experimental Investigation for Selection of Unloading Criterion in Multistage Triaxial Testing. ARMA 21–1217, *55th US Rock Mechanics/Geomechanics Symposium* held in Houston, Texas, USA, 20-23 June 2021. (2021).
30. R. Span and W. Wagner. A new equation of state for CO_2 covering the fluid region from the triple point temperature to 1100K at pressures upto 800MPa. *J. Phys. Chem. Ref. Data* Vol. **25**, No 6 (1996).
31. M. Batzle and Z. Wang. Seismic properties of pore fluids. *GEOPHYSICS*, VOL. **57**, NO. 11 P. 1396-1408 (1992).
32. P.J. Linstrom and W.G. Mallard, Eds., NIST Chemistry WebBook, *NIST Standard Reference Database Number* **69**,National Institute of Standards and Technology, Gaithersburg MD, 20899, https://doi.org/10.18434/T4D303, (retrieved July 4, 2022)